

NexusSplats: Efficient 3D Gaussian Splatting in the Wild

Yuzhou Tang Dejun Xu Yongjie Hou Zhenzhong Wang Min Jiang[†]

School of Informatics, Xiamen University

<https://nexus-splats.github.io/>

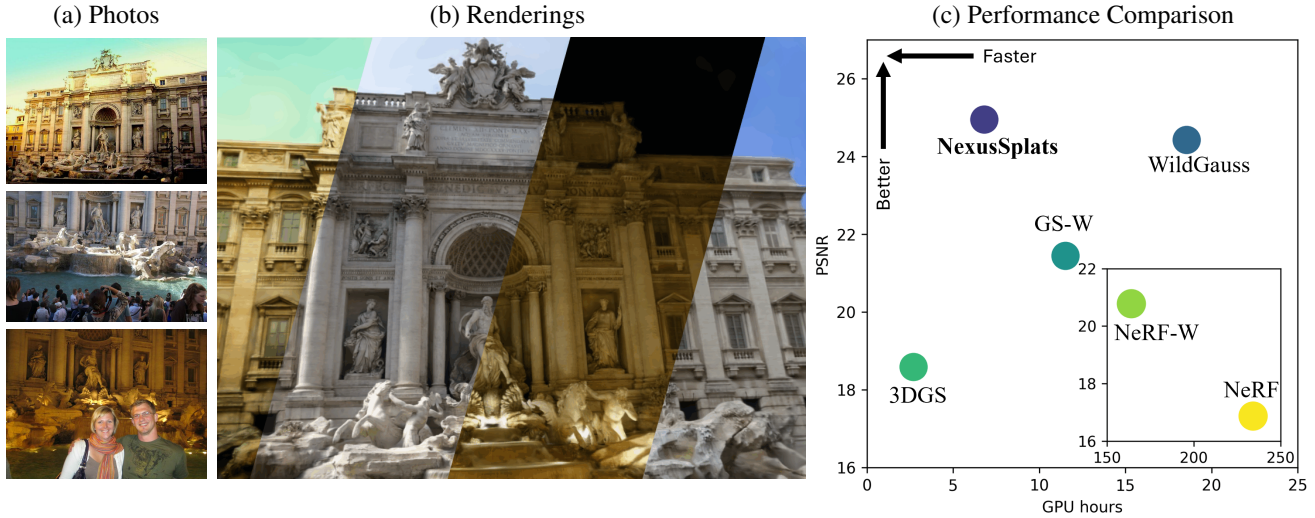


Figure 1. (a) Given photos from *in-the-wild* scenarios, (b) our method decouples lighting conditions and eliminates occlusions, enabling steerable color mapping to diverse lighting conditions. (c) **NexusSplats** achieves state-of-the-art rendering quality, with a substantial training speed improvement over extensions of 3DGS.

Abstract

Photorealistic 3D reconstruction of unstructured real-world scenes remains challenging due to complex illumination variations and transient occlusions. Existing methods based on Neural Radiance Fields (NeRF) and 3D Gaussian Splatting (3DGS) struggle with inefficient light decoupling and structure-agnostic occlusion handling. To address these limitations, we propose NexusSplats, an approach tailored for efficient and high-fidelity 3D scene reconstruction under complex lighting and occlusion conditions. In particular, NexusSplats leverages a hierarchical light decoupling strategy that performs centralized appearance learning, efficiently and effectively decoupling varying lighting conditions. Furthermore, a structure-aware occlusion handling mechanism is developed, establishing a nexus between 3D and 2D structures for fine-grained occlusion handling. Experimental results demonstrate that NexusSplats achieves state-of-the-art rendering quality and reduces the number of total parameters by 65.4%, leading

to $2.7\times$ faster reconstruction.

1. Introduction

Photorealistic 3D scene reconstruction from unstructured image collections remains a cornerstone for applications ranging from virtual reality to autonomous navigation [4, 21]. While Neural Radiance Fields (NeRFs) [1, 23, 30, 38] achieve impressive view synthesis in controlled settings, their volumetric rendering struggles with *in-the-wild* scenarios characterized by illumination variations (e.g. weather changes) and transient occlusions (e.g. moving pedestrians). NeRF-W [21] pioneers light decoupling and occlusion handling through image-specific appearance and transient embeddings combined with color mapping and 2D uncertainty estimation. Follow-up works [4, 11, 16, 32, 44] enhance the appearance and uncertainty modeling by introducing various image feature extractors, such as CNN and U-Net. However, these methods inherit NeRF’s prohibitive computational cost, requiring hours of training per scene.

The emergence of 3D Gaussian Splatting (3DGS) [12, 45, 46] revolutionizes the field with explicit 3D Gaus-

[†]Corresponding author.

sians and differentiable rasterization [49], enabling faster reconstruction with real-time rendering. Recent adaptations [14, 41, 42, 47] extend 3DGS to *in-the-wild* scenes by introducing per-Gaussian appearance embeddings and scattered color mapping to decouple lighting conditions from each explicit Gaussian primitive. To handle transient occlusions, these methods remain their focus on advanced image feature extractors for uncertainty modeling.

Despite progress in improving rendering quality, two fundamental limitations persist: (1) **Inefficient light decoupling**. Representing outdoor scenes with millions of 3D Gaussians, current methods attach independent appearance embeddings to the substantial number of Gaussians. This scattered appearance learning increases the total number of parameters and slows training, while simplified alternatives like positional encodings [6] sacrifice texture fidelity due to insufficient learning of detailed appearance features. (2) **Structure-agnostic occlusion handling**. Existing 2D-centric occlusion detection fails to account for the inherent structural discrepancies between 2D input images and the 3D representation, limiting the accuracy in capturing occlusions. Besides, clear scene boundaries where no occlusions appear are frequently misclassified as occlusions by existing methods. Excluding clear areas while retaining uncaptured occlusions leads to incomplete scene reconstruction with artifacts and shadows.

The key to addressing these issues lies in two key perspectives: (1) Construct an efficient structure that learns sufficient appearance details while scaling down the parameters. (2) Build a nexus between 3D and 2D structures to enable more accurate occlusion captures. Based on this, we propose **NexusSplats** that performs hierarchical light decoupling and structure-aware occlusion handling.

To enable hierarchical light decoupling, we introduce the hierarchical and region-aware 3D representation [20] to organize the 3D Gaussians into *nexus kernels* — dynamic 3D primitives tailored for *in-the-wild* scene reconstruction. In particular, each *nexus kernel* learns a shared appearance embedding and coordinates color mapping for its managed Gaussians, allowing for centralized appearance learning while scaling down the number of appearance embeddings. This design maintains sufficient detail learning and ensures rendering quality. Regarding occlusion handling, a shared uncertainty embedding is also assigned for each kernel to predict the 3D uncertainties of the associated Gaussians. These 3D uncertainties are then projected onto image planes via tile rasterization, propagating to 2D uncertainty masks. To further correct misidentifications on clear scene boundaries, we apply a boundary-aware refinement to the 2D uncertainty masks. Combined with the 2D semantic feature loss [14, 31], our uncertainty propagation mechanism bridges 3D uncertainties with 2D semantic features, improving the accuracy of capturing true occlusions. Ex-

tensive experiments demonstrate that our method not only significantly reduces redundant parameters but also presents finer textures and a more accurate removal of occlusions.

In summary, our key contributions are as follows:

- We develop a hierarchical light decoupling strategy that performs centralized appearance learning, efficiently and effectively decoupling varying lighting conditions.
- We design a structure-aware occlusion handling mechanism that establishes a nexus between 3D and 2D structures, improving the accuracy of occlusion captures.
- Experimental results demonstrate that NexusSplats achieves state-of-the-art rendering quality and reduces total parameters by 65.4%, which leads to $2.7\times$ faster reconstruction.

2. Related Work

2.1. Novel View Synthesis

NeRFs [1, 23, 30, 38] revolutionize 3D scene reconstruction through continuous volumetric representations, enabling photorealistic novel view synthesis. However, their reliance on ray tracing and MLP-based rendering imposes prohibitive computational costs [5, 22, 29]. Subsequent works accelerate NeRFs through enhanced scene representations [3, 8, 12, 19, 25, 37], where 3DGS [12, 45, 46] excels in its remarkable efficiency without compromising rendering quality by combining explicit 3D Gaussians with differentiable rasterization. While follow-up works [7, 15, 17, 20, 24, 26, 27] further compress 3DGS representations for settling large-scale scenes, they remain inadequate in handling real-world challenges like complex illumination variations and transient occlusions. In this paper, we investigate scene representations tailored for such challenging conditions.

2.2. Lighting Condition Decoupling

To handle illumination variations, NeRF-based methods [4, 11, 16, 21, 32, 44] typically employ image-specific embeddings and neural feature extractors to disentangle appearance changes. However, these approaches inherit NeRF’s computational inefficiency, resulting in prohibitive training and rendering times. Recent efforts [14, 41, 42, 47] integrate appearance conditioning with 3DGS by introducing per-Gaussian appearance embeddings and scattered color mapping. Though proven to be effective, optimizing such a substantial number of extra parameters significantly increases computational costs. While SWAG [6] proposes positional encodings to replace per-Gaussian embeddings for higher efficiency, this strategy sacrifices texture fidelity due to limited appearance modeling capacity. Our approach strikes a novel balance between efficiency and quality by introducing a hierarchical light decoupling strategy that maintains high-fidelity rendering without excessive parameters.

2.3. Transient Occlusion Handling

To mitigate the impact of transient occlusions, such as moving pedestrians and vehicles, pioneering works [4, 21, 33, 44] either predict 2D uncertainty masks or leverage loss controls based on image feature extractors (e.g. CNN and U-Net) to capture and eliminate occlusions, thereby preventing their models from learning irrelevant objects from training images. Subsequent methods [14, 31] enhance occlusion detection using advanced semantic feature extractors like DINO [2, 28]. However, their reliance on 2D-informed guidance can lead to inconsistencies with the underlying 3D scene geometry, making them more prone to occasional false or missed occlusion identifications. In addition, specialized 3DGS variants for occlusion handling [18, 34] primarily focus on small-scale indoor scenarios, which involve occlusion challenges but lack drastic illumination variations in real-world outdoor environments. In contrast, our method introduces a structure-aware occlusion handling framework designed for large outdoor scenes, where complex illumination changes and transient objects coexist. This dual consideration of lighting and occlusion distinguishes our approach from existing solutions that address transient occlusions in isolation.

3. Methods

Figure 2 illustrates our approach, NexusSplats, an approach addressing inefficient light decoupling and structure-agnostic occlusion handling in unstructured 3D scene reconstruction. Our approach comprises two key components: (1) **Hierarchical Light Decoupling** (Section 3.2) that leverages *nexus kernels* to hierarchically manage 3D Gaussians and perform centralized appearance learning for efficient and effective light condition decoupling. (2) **Structure-Aware Occlusion Handling** (Section 3.3) that bridges 3D uncertainties with 2D semantic features via uncertainty propagation and incorporates the boundary-aware refinement to mitigate misclassifications at scene boundaries. Using a combination of color loss and uncertainty loss, NexusSplats enables delicate scene reconstructions with steerable lighting conditions via unified optimization (Section 3.4). In this section, we detail each component of NexusSplats, elaborating on how they collectively contribute to efficient and high-quality 3D scene reconstruction under complex conditions.

3.1. Preliminaries

In this section, we briefly review 3DGS [12] and its extension Scaffold-GS [20], which jointly serve as a basis of our approach. These methods combine explicit 3D Gaussian representations with differentiable rasterization for efficient scene reconstruction.

3D Gaussian Splatting represents scenes using anisotropic 3D Gaussians initialized from Structure-from-Motion (SfM) point clouds [35]. Each Gaussian $\mathcal{G}(\mathbf{x})$ is defined by:

$$\mathcal{G}(\mathbf{x}) = e^{-\frac{1}{2}(\mathbf{x}-\mu)^\top \Sigma^{-1}(\mathbf{x}-\mu)}, \quad \Sigma = \mathbf{R}\mathbf{S}\mathbf{S}^\top \mathbf{R}^\top, \quad (1)$$

where μ is the centroid position of a 3D Gaussian, and Σ encodes anisotropic covariance via a scaling matrix \mathbf{S} and a rotation matrix \mathbf{R} . Each Gaussian also stores the view-dependent color $\hat{\mathbf{c}}$, modeled by spherical harmonics, and an opacity α .

Unlike traditional volumetric methods, 3DGS uses tile-based rasterization [49] for real-time rendering. Each 3D Gaussian $\mathcal{G}(\mathbf{x})$ is projected onto image planes, resulting in a 2D Gaussian $\mathcal{G}'(\mathbf{x}')$. The 2D Gaussians are then sorted and splatted via α -blending:

$$\hat{\mathbf{C}}(\mathbf{x}') = \sum_{i \in N} \hat{\mathbf{c}}_i \sigma_i \prod_{j=1}^{i-1} (1 - \sigma_j), \quad \sigma_i = \alpha_i \mathcal{G}'_i(\mathbf{x}'), \quad (2)$$

where σ_i denotes the contribution weight of the i -th Gaussian to pixel \mathbf{x}' . With the differentiable property, all attributes of 3D Gaussians are learnable and optimized end-to-end during training.

Scaffold-GS introduces a hierarchical representation to address parameter redundancy in large-scale scenes. Instead of directly optimizing a large, unstructured set of Gaussians, Scaffold-GS organizes the scene using a sparse grid of anchor points $\{\mathcal{V}_i\}$, initialized from SfM point clouds and dynamically generating h neural Gaussians per anchor:

$$\{\mu_j\}_{j=1}^h = \mathbf{x}_i + \{\mathcal{O}_j\}_{j=1}^h \cdot l_v, \quad (3)$$

where \mathbf{x}_i is the position of anchor \mathcal{V}_i , and $\{\mathcal{O}_j\}$ and l_v are learnable offsets and scaling factors.

To generate the attributes of each neural Gaussian, Scaffold-GS employs respective MLPs for prediction. Notably, the spherical harmonics with dynamic color channels are replaced with neural networks with fixed channels, consistent with other Gaussian attributes. Specifically, given viewing position \mathbf{x}_v , anchor \mathcal{V}_i predicts the colors $\{\hat{\mathbf{c}}_j\}_{j=1}^h$ of neural Gaussians by:

$$\{\hat{\mathbf{c}}_j\}_{j=1}^h = F_c(\mathbf{f}_v, \vec{d}_{iv}), \quad \vec{d}_{iv} = \frac{\mathbf{x}_i - \mathbf{x}_v}{\|\mathbf{x}_i - \mathbf{x}_v\|_2}, \quad (4)$$

where F_c is the color MLP shared by all anchors and the viewing direction \vec{d}_{iv} ensures viewing consistency. Analogous MLPs, F_α , F_q , and F_s , are used for opacity, covariance matrix, and scaling prediction. Finally, a unique optimization process is developed to prune redundant anchors with associated neural Gaussians and reduce total parameters.

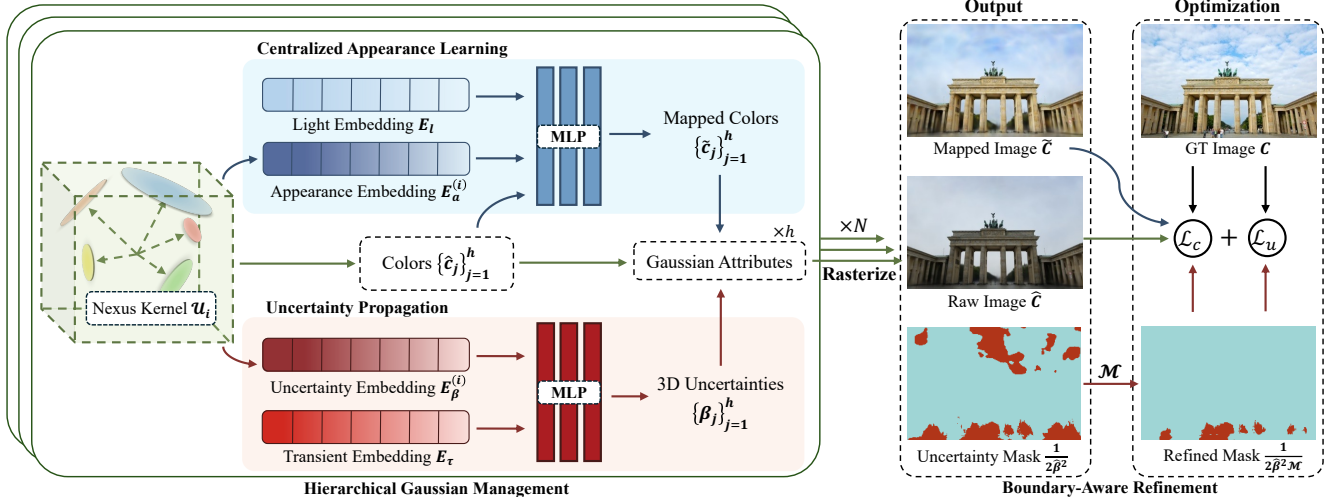


Figure 2. **Overview of NexusSplats.** Our framework operates in three stages: *First*, the hierarchical Gaussian management (Section 3.2.1) organizes 3D Gaussians into dynamic *nexus kernels*, which generate Gaussian attributes and perform centralized appearance learning (Section 3.2.2) and uncertainty propagation (Section 3.3.1). *Second*, a raw image \hat{C} , a mapped image \tilde{C} , and an uncertainty mask $\frac{1}{2\beta^2}$ are rendered through tile rasterization. *Third*, the boundary-aware refinement (Section 3.3.2) corrects misclassified scene boundaries. The system optimizes via a combination of color loss \mathcal{L}_c and uncertainty loss \mathcal{L}_u .

3.2. Hierarchical Light Decoupling

This section introduces our hierarchical light decoupling strategy that consists of hierarchical Gaussian management and centralized appearance learning. This design effectively reduces parameter redundancy while achieving superior texture fidelity under varying illumination.

3.2.1. Hierarchical Gaussian Management

The core objective of hierarchical light decoupling is to establish an efficient representation that learns sufficient appearance features across 3D Gaussians while minimizing parameter overhead. A natural strategy involves reducing the number of appearance embeddings by grouping spatially adjacent Gaussians with similar appearance characteristics. However, roughly clustering Gaussian primitives based on their positions and colors suffers from two critical limitations.

First, leveraging a static clustering approach, where 3D Gaussians are roughly grouped based on their initial positions and colors, fails to capture the dynamic changes in Gaussian attributes (e.g. position, opacity, color) during training, leading to inconsistent appearance groupings. Second, introducing dynamic clustering requires frequent re-clustering which incurs prohibitive computational costs due to pairwise similarity calculations across millions of Gaussians.

To address these challenges, we draw inspiration from the hierarchical organization strategy of Scaffold-GS [20] and utilize it for Gaussian management. Expanding on the concept of anchor points, we introduce *nexus kernels*, which inherit the neural Gaussian generation capability and learn

detailed appearance features in a centralized manner. In this way, each *nexus kernel* ensures the appearance similarities of the neural Gaussians it spawns, paving the way for centralized appearance learning.

3.2.2. Centralized Appearance Learning

Equipped with the shared appearance embedding $\varepsilon_a^{(i)}$, each *nexus kernel* U_i learns centralized appearance features and coordinates color mapping for its h constituent Gaussians through a shared lighting-sensitive MLP F_θ :

$$\{\tilde{c}_j\}_{j=1}^h = F_\theta(\{\hat{c}_j\}_{j=1}^h, \varepsilon_a^{(i)}, \varepsilon_l^{(v)}, \vec{d}_{iv}), \quad (5)$$

where $\varepsilon_l^{(v)}$ is the view-specific light embedding from input image C_v , following previous literature [6, 14, 21]. To maintain view consistency after color mapping, we also input the viewing direction \vec{d}_{iv} into F_θ , aligned with the raw color prediction process (Eq. (4)). Through tile rasterization, both raw colors \hat{c} and mapped colors \tilde{c} are projected onto image planes for loss computation.

By binding color transformations to kernel-level appearance embeddings rather than individual Gaussians, our method not only accelerates convergence through parameter sharing but also enhances representational capacity by facilitating appearance embeddings $\{\varepsilon_a^{(i)}\}$ to encode material-aware illumination responses and structural coherence. This centralized paradigm contrasts sharply with conventional scattered embedding approaches, where isolated per-Gaussian parameters struggle to capture non-local lighting effects. Critically, the fixed-channel color expression provides a more stable optimization landscape compared to

spherical harmonics with dynamic channels that are incompatible with neural network-based color mapping.

3.3. Structure-Aware Occlusion Handling

This section elaborates on our structure-aware occlusion handling framework that bridges 2D uncertainty estimation with 3D representations to improve the accuracy of occlusion captures. In particular, our design leverages the 3D uncertainty estimation that grounds occlusion reasoning in geometric primitives and boundary-aware refinement that resolves semantic inconsistencies at scene peripheries.

3.3.1. Uncertainty Propagation

Central to this design is the prediction of 3D uncertainties $\{\beta_i\}$ for individual Gaussians through *nexus kernels*. Learning an uncertainty embedding $\varepsilon_\beta^{(i)}$, each *nexus kernel* \mathcal{U}_i produces per-Gaussian confidence scores through a shared MLP F_β :

$$\{\beta_j\}_{j=1}^h = F_\beta(\varepsilon_\beta^{(i)}, \varepsilon_\tau^{(v)}), \quad (6)$$

where ε_τ is the transient embedding for recording image-specific occlusion patterns. These 3D uncertainties $\{\beta_i\}$ are projected onto 2D image planes via tile rasterization:

$$\hat{\beta}(\mathbf{x}') = \sum_{j \in h \times N} \beta_j \sigma_j \prod_{k=1}^{j-1} (1 - \sigma_k), \quad (7)$$

where $\hat{\beta}(\mathbf{x}')$ denotes the 2D uncertainty of pixel \mathbf{x}' and σ_j follows the same blending weights as color rendering (Equation (2)).

This uncertainty propagation mechanism effectively suppresses false positives in textureless regions by grounding occlusion reasoning in geometric confidences derived from the 3D representation, enabling robust occlusion segmentation in complex outdoor scenes with dynamic lighting and transient objects.

3.3.2. Boundary-Aware Refinement

Due to the lack of observations in training sets, the scene boundaries of the 3D representation often present lower rendering quality, leading to semantic discrepancies between rendered and ground-truth images and misclassifications by image models.

To address the misclassifications at scene boundaries, we introduce a boundary-aware refinement modeled as an anisotropic 2D Gaussian distribution:

$$\mathcal{M}(\mathbf{x}') = e^{-\frac{1}{2}(\mathbf{x}' - \mu')^\top \Sigma^{-1}(\mathbf{x}' - \mu')}, \quad (8)$$

where μ' and Σ are estimated via DINO [28] features, determining the rough scope of the foreground of input images. This refinement modulates uncertainty values near scene peripheries, reducing sensitivity in ambiguous regions while preserving occlusion accuracy in well-observed areas.

3.4. Unified Optimization

Our training objective integrates a color loss \mathcal{L}_c and an uncertainty loss \mathcal{L}_u to jointly optimize geometry, appearance, and uncertainty reasoning. The color loss combines structural and perceptual similarity metrics through a weighted sum of DSSIM [40] and L_1 losses, dynamically modulated by predicted uncertainty mask $\frac{1}{2\hat{\beta}^2\mathcal{M}}$ to attenuate contributions from occluded regions:

$$\mathcal{L}_c = \frac{\lambda}{2\hat{\beta}^2\mathcal{M}} \text{DSSIM}(\hat{\mathbf{C}}, \mathbf{C}) + \frac{1-\lambda}{2\hat{\beta}^2\mathcal{M}} L_1(\hat{\mathbf{C}}, \mathbf{C}), \quad (9)$$

where λ is set to 0.2 as a hyper-parameter. The uncertainty loss \mathcal{L}_u enhances occlusion sensitivity through a hybrid formulation:

$$\mathcal{L}_u = \frac{\mathcal{D}(\hat{\mathbf{C}}, \mathbf{C})}{2\hat{\beta}^2} + \lambda_1 \log \hat{\beta}, \quad (10)$$

where $\mathcal{D}(\cdot)$ measures cosine similarity between DINO [28] features of rendered and ground-truth images, and $\lambda_1 = 0.5$ controls the trade-off between uncertainty regulation and semantic consistency.

4. Experiments

4.1. Experimental Setup

Datasets and Metrics. We evaluate NexusSplats on the Photo Tourism dataset [36], a standard benchmark for *in-the-wild* 3D reconstruction featuring scenes with illumination changes and transient occlusions. For occlusion handling analysis, we extend evaluations to the NeRF On-the-go dataset [31], which provides urban scenes with varying ratios of occlusions. Efficiency comparisons are conducted solely on Photo Tourism, primarily because scenes in the NeRF On-the-Go dataset lack significant lighting variations, and most baseline approaches do not incorporate light decoupling modules when reconstructing such scenes. Metrics include PSNR, SSIM [40], and LPIPS [48] for rendering quality, alongside training time (GPU hours) and rendering speed (FPS).

Baselines and Implementation. To ensure rigorous and reproducible evaluation, we benchmark our method against open-source methods addressing *in-the-wild* novel view synthesis: NeRF variants (NeRF [23], NeRF-W [21], K-Planes [9]) and 3DGS-based approaches (3DGS [12], GS-W [47], WildGauss [14]). Methods without public implementations (e.g. Wild-GS [42], SWAG [6]) are excluded to mitigate potential implementation biases and ensure consistency across evaluations. All baselines are retrained under their official configurations on a single NVIDIA A40 GPU for 200k iterations, following NeRF-W’s evaluation protocol [13, 21] (embedding optimization on test-image left halves). Additional implementation details are provided in Appendix A.

Table 1. **Quantitative Comparison** on the Photo Tourism dataset [36]. Highlighted values indicate the **first**, **second**, and **third** scores for each metric and scene.

Method	Brandenburg Gate			Sacre Coeur			Trevi Fountain			Mean Efficiency	
	PSNR \uparrow	SSIM \uparrow	LPIPS \downarrow	PSNR \uparrow	SSIM \uparrow	LPIPS \downarrow	PSNR \uparrow	SSIM \uparrow	LPIPS \downarrow	GPU hrs. \downarrow	FPS \uparrow
NeRF [23]	18.90	0.815	0.231	15.60	0.715	0.291	16.14	0.600	0.366	>100	<1
NeRF-W-re [21]	24.17	0.890	0.167	19.20	0.807	0.191	18.97	0.698	0.265	>100	<1
K-Planes [9]	25.49	0.879	0.224	20.61	0.774	0.265	22.67	0.714	0.317	1.58	<1
3DGS [12]	19.50	0.871	0.177	17.44	0.836	0.201	17.75	0.706	0.279	1.93	11.6
GS-W [47]	24.32	0.909	0.148	19.57	0.826	0.207	20.48	0.734	0.252	11.52	10.0
WildGauss [14]	27.23	0.926	0.135	22.56	0.859	0.177	23.52	0.765	0.228	18.54	7.5
Ours	27.76	0.922	0.141	23.13	0.859	0.174	23.97	0.766	0.237	6.81	11.5
w/o light.	20.31	0.880	0.194	17.08	0.816	0.224	17.92	0.701	0.316	6.73	15.0
w/o uncert.	27.12	0.924	0.143	22.61	0.857	0.180	23.92	0.761	0.253	5.96	13.9
w/o refine.	26.79	0.922	0.143	22.33	0.857	0.178	23.81	0.766	0.244	6.54	11.5

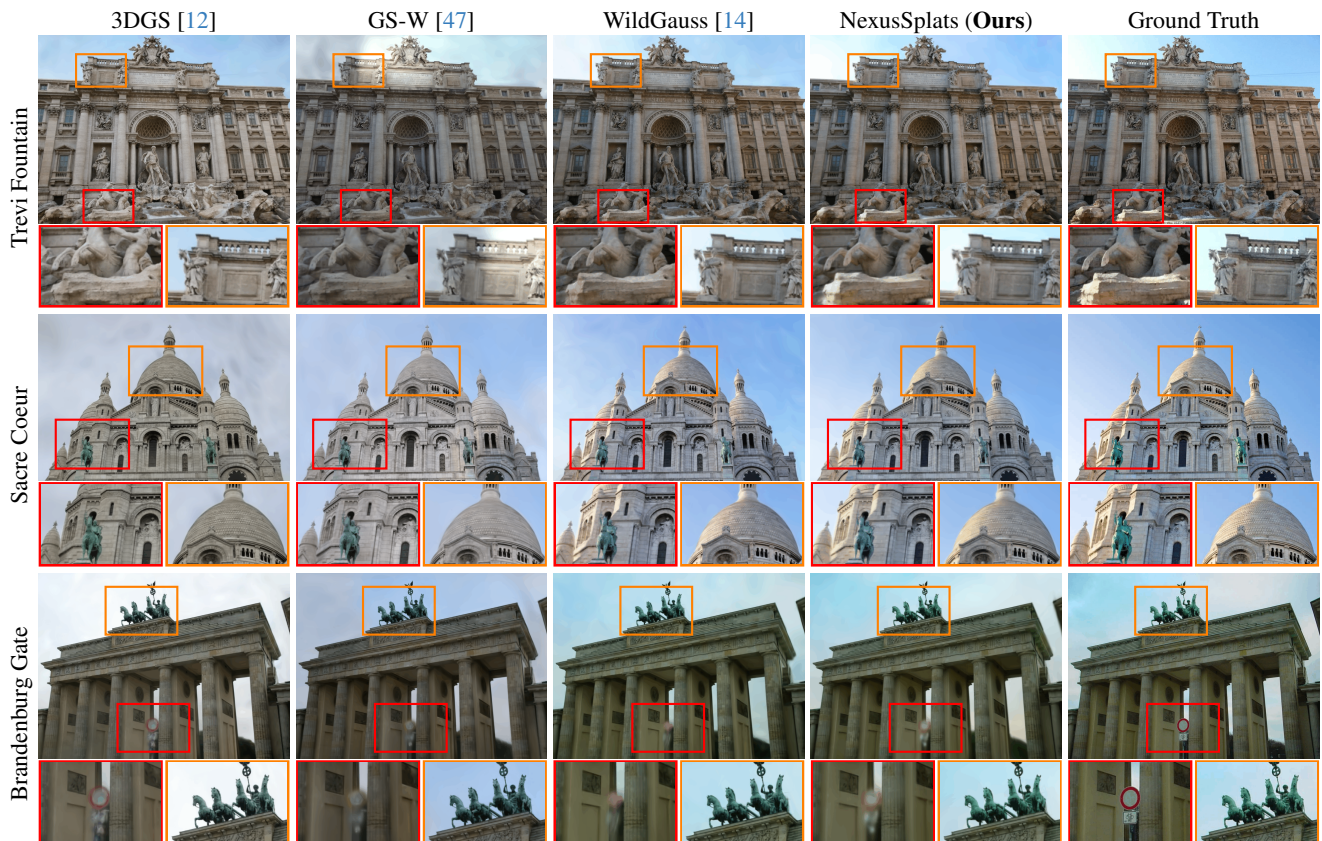


Figure 3. **Qualitative Comparison** on the Photo Tourism dataset [36]. For each row, different architectural scenes are shown with highlighted red and orange boxes for closer inspection. NexusSplats presents sharper details and improved color fidelity, closely matching the ground truth images, particularly in challenging areas with intricate textures.

4.2. Evaluations

Comparisons on Photo Tourism. We conduct comprehensive evaluations on the Photo Tourism dataset to assess rendering quality and efficiency under real-world conditions. Quantitative comparisons in Table 1 demonstrate

that NexusSplats achieves state-of-the-art rendering quality while presenting competitive training and rendering speed. Moreover, the qualitative comparison in Figure 3 further showcases that our method preserves finer-grained details in adapting to varying lighting conditions, which corresponds the closest to the ground truth.



Figure 4. **Qualitative Comparison** on the NerRF On-the-go dataset [31]. We present the results of three scenes with different ratios of occlusions. Our method removes all occlusions and shows the best view synthesis results.

Table 2. **Efficiency Comparison** across three Photo Tourism scenes [36]. Metrics include the number of appearance embeddings (AE), total parameters (TP), training time (TT) in GPU hours, and rendering quality (PSNR). The first, second, and third values are highlighted.

Method	AE ↓	TP ↓	TT ↓	PSNR ↑
3DGS [12]	-	54.3M	1.93	18.23
GS-W [47]	260K	21.6M	11.52	21.46
WildGauss [14]	927K	77.1M	18.54	24.44
Ours	192K	26.7M	6.81	24.95

Comparisons on NeRF On-the-go. To validate generalization capabilities, we evaluate NexusSplats on the NeRF On-the-go dataset, which features urban scenes with transient objects. The qualitative results in Figure 4 demonstrate that our method successfully ignores occlusions while reconstructing static scenes across different ratios of occlusions, while other baselines incorporate transient shadows into the scene geometry at different levels. Remaining qualitative and quantitative comparisons on NeRF On-the-go are provided in Appendix B.

Efficiency Comparison. As shown in Table 2, NexusSplats reduces the number of appearance embeddings by 79.3% compared to WildGauss [14], demonstrating the parameter efficiency of kernel-level centralized appearance learning. Despite using 65.4% fewer total parameters than WildGauss, we achieve the highest PSNR. Notably, the training time is reduced by 63.2%, proving that our hierarchical light decoupling strategy avoids the substantial computational cost of per-Gaussian processing. Although GS-W [47] attains lower total parameters, its PSNR drops by 16.3%, revealing a trade-off between accuracy and efficiency. These results validate that hierarchical management enabled by nexus kernels enhances computational efficiency without damaging the fidelity of reconstruction in complex *in-the-wild* scenarios.

4.3. Ablation Study and Analysis

To isolate the contributions of our core innovations, we systematically ablate our core modules on the Photo Tourism dataset. As shown in Table 1, disabling the **hierarchical light decoupling** module causes a severe performance drop, primarily due to unmodeled lighting variations corrupting



Figure 5. **Light Decoupling Visualizations** on Photo Tourism [36]. NexusSplats maps colors from the reconstructed scene to match the target lighting conditions from ground truth images.

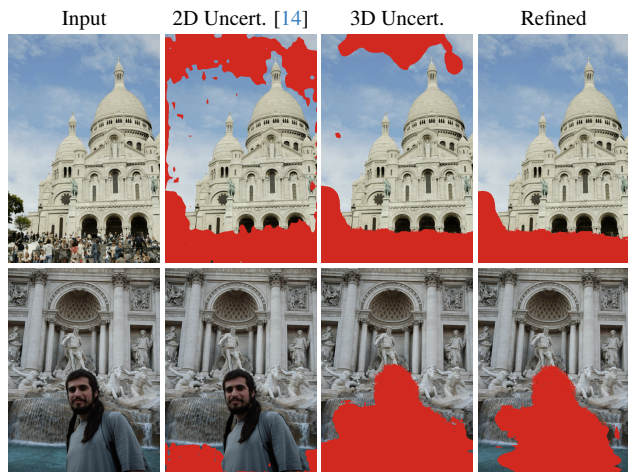


Figure 6. **Occlusion Handling Visualizations** on Photo Tourism [36]. The red masks denote uncertainty predictions by different modelings.

material appearances. Removing the **structure-aware occlusion handling** module degrades reconstruction quality as transient objects pollute the static scene representation. Notably, omitting the **boundary-aware refinement** disproportionately impacts PSNR, as over-suppression of boundary regions introduces insufficient reconstruction. The full framework achieves optimal balance, where centralized appearance learning preserves high-frequency textures, 3D uncertainty propagation filters transient occlusions, and boundary relaxation prevents potential harm to the overall reconstruction.

Light Decoupling Visualizations. Figure 5 illustrates the capability of our method to decouple and adapt to varying lighting conditions. Six distinct lighting conditions from the Trevi Fountain scene, captured at different times and under various ambient lighting scenarios, serve as the target lighting conditions. NexusSplats successfully maps scene colors to these target lighting conditions across three viewpoints, demonstrating its resilience to illumination variations while maintaining color consistency and detail integrity.

Occlusion Handling Visualizations. Figure 6 showcases the improved performance in capturing occlusions of the 3D uncertainty mechanism over 2D uncertainty modeling. Furthermore, without boundary-aware refinement, our method also occasionally misidentifies clear boundary areas, such as the sky and water, as occlusions. Incorporating the refinement improves the overall performance in handling occlusions, mitigating the drawbacks of uncertainty modeling. Further ablations and visualizations can be found in Appendix C.

5. Conclusion

In this work, we introduced NexusSplats, an efficient framework for high-fidelity 3D scene reconstruction under complex lighting and occlusion conditions. By introducing hierarchical light decoupling, our method centralizes appearance learning through hierarchical Gaussian management, significantly reducing the number of parameters and accelerating training while preserving texture fidelity. The proposed structure-aware occlusion pipeline bridges 3D and 2D structural discrepancies via uncertainty propagation and boundary-aware refinement, eliminating persistent artifacts

in prior works. Experimental results validate the superiority of NexusSplats in both efficiency and reconstruction quality. Our approach marks a critical step toward practical, high-fidelity 3D reconstruction for real-world applications.

References

- [1] Jonathan T Barron, Ben Mildenhall, Dor Verbin, Pratul P Srinivasan, and Peter Hedman. Mip-nerf 360: Unbounded anti-aliased neural radiance fields. In *CVPR*, pages 5470–5479, 2022. 1, 2
- [2] Mathilde Caron, Hugo Touvron, Ishan Misra, Hervé Jégou, Julien Mairal, Piotr Bojanowski, and Armand Joulin. Emerging properties in self-supervised vision transformers. In *CVPR*, pages 9650–9660, 2021. 3
- [3] Anpei Chen, Zexiang Xu, Andreas Geiger, Jingyi Yu, and Hao Su. Tensorf: Tensorial radiance fields. In *ECCV*, pages 333–350. Springer, 2022. 2
- [4] Xingyu Chen, Qi Zhang, Xiaoyu Li, Yue Chen, Ying Feng, Xuan Wang, and Jue Wang. Hallucinated neural radiance fields in the wild. In *CVPR*, pages 12943–12952, 2022. 1, 2, 3
- [5] Zhiqin Chen and Hao Zhang. Learning implicit fields for generative shape modeling. In *CVPR*, pages 5939–5948, 2019. 2
- [6] Hiba Dahmani, Moussab Bennehar, Nathan Piasco, Luis Roldao, and Dzmityr Tsishkou. Swag: Splatting in the wild images with appearance-conditioned gaussians. In *ECCV*, pages 325–340. Springer, 2024. 2, 4, 5, 1
- [7] Zhiwen Fan, Kevin Wang, Kairun Wen, Zehao Zhu, De-jia Xu, and Zhangyang Wang. Lightgaussian: Unbounded 3d gaussian compression with 15x reduction and 200+ fps. *NeurIPS*, 2024. 2
- [8] Sara Fridovich-Keil, Alex Yu, Matthew Tancik, Qinlong Chen, Benjamin Recht, and Angjoo Kanazawa. Plenoxels: Radiance fields without neural networks. In *CVPR*, pages 5501–5510, 2022. 2
- [9] Sara Fridovich-Keil, Giacomo Meanti, Frederik Rahbæk Warburg, Benjamin Recht, and Angjoo Kanazawa. K-planes: Explicit radiance fields in space, time, and appearance. In *CVPR*, pages 12479–12488, 2023. 5, 6
- [10] Kaiming He, Xinlei Chen, Saining Xie, Yanghao Li, Piotr Dollár, and Ross Girshick. Masked autoencoders are scalable vision learners. In *CVPR*, pages 16000–16009, 2022. 5
- [11] Karim Kassab, Antoine Schnepf, Jean-Yves Franceschi, Laurent Caraffa, Jeremie Mary, and Valérie Gouet-Brunet. Refinedfields: Radiance fields refinement for unconstrained scenes. *arXiv preprint arXiv:2312.00639*, 2023. 1, 2
- [12] Bernhard Kerbl, Georgios Kopanas, Thomas Leimkühler, and George Drettakis. 3d gaussian splatting for real-time radiance field rendering. *ACM TOG*, 42(4):139–1, 2023. 1, 2, 3, 5, 6, 7
- [13] Jonas Kulhanek and Torsten Sattler. Nerfbaselines: Consistent and reproducible evaluation of novel view synthesis methods. *arXiv preprint arXiv:2406.17345*, 2024. 5, 1
- [14] Jonas Kulhanek, Songyou Peng, Zuzana Kukelova, Marc Pollefeys, and Torsten Sattler. Wildgaussians: 3d gaussian splatting in the wild. *NeurIPS*, 2024. 2, 3, 4, 5, 6, 7, 8, 1
- [15] Joo Chan Lee, Daniel Rho, Xiangyu Sun, Jong Hwan Ko, and Eunbyung Park. Compact 3d gaussian representation for radiance field. In *CVPR*, pages 21719–21728, 2024. 2
- [16] Peihao Li, Shaohui Wang, Chen Yang, Bingbing Liu, Weichao Qiu, and Haoqian Wang. Nerf-ms: Neural radiance fields with multi-sequence. In *ICCV*, pages 18591–18600, 2023. 1, 2
- [17] Jiaqi Lin, Zhihao Li, Xiao Tang, Jianzhuang Liu, Shiyong Liu, Jiayue Liu, Yangdi Lu, Xiaofei Wu, Songcen Xu, Youliang Yan, et al. Vastgaussian: Vast 3d gaussians for large scene reconstruction. In *CVPR*, pages 5166–5175, 2024. 2
- [18] Jingyu Lin, Jiaqi Gu, Lubin Fan, Bojian Wu, Yujing Lou, Renjie Chen, Ligang Liu, and Jieping Ye. Hybridgs: Decoupling transients and statics with 2d and 3d gaussian splatting. In *CVPR*, 2025. 3
- [19] Lingjie Liu, Jiatao Gu, Kyaw Zaw Lin, Tat-Seng Chua, and Christian Theobalt. Neural sparse voxel fields. *NeurIPS*, 33: 15651–15663, 2020. 2
- [20] Tao Lu, Mulin Yu, Linning Xu, Yuanbo Xiangli, Limin Wang, Dahua Lin, and Bo Dai. Scaffold-gs: Structured 3d gaussians for view-adaptive rendering. In *CVPR*, pages 20654–20664, 2024. 2, 3, 4, 1
- [21] Ricardo Martin-Brualla, Noha Radwan, Mehdi SM Sajjadi, Jonathan T Barron, Alexey Dosovitskiy, and Daniel Duckworth. Nerf in the wild: Neural radiance fields for unconstrained photo collections. In *CVPR*, pages 7210–7219, 2021. 1, 2, 3, 4, 5, 6
- [22] Lars Mescheder, Michael Oechsle, Michael Niemeyer, Sebastian Nowozin, and Andreas Geiger. Occupancy networks: Learning 3d reconstruction in function space. In *CVPR*, pages 4460–4470, 2019. 2
- [23] Ben Mildenhall, Pratul P Srinivasan, Matthew Tancik, Jonathan T Barron, Ravi Ramamoorthi, and Ren Ng. Nerf: Representing scenes as neural radiance fields for view synthesis. *ECCV*, 65(1):99–106, 2021. 1, 2, 5, 6
- [24] Wieland Morgenstern, Florian Barthel, Anna Hilsmann, and Peter Eisert. Compact 3d scene representation via self-organizing gaussian grids. *ECCV*, 2023. 2
- [25] Thomas Müller, Alex Evans, Christoph Schied, and Alexander Keller. Instant neural graphics primitives with a multiresolution hash encoding. *ACM TOG*, 41(4):1–15, 2022. 2
- [26] KL Navaneet, Kossar Pourahmadi Meibodi, Sorous Abbasi Koohpayegani, and Hamed Pirsavash. Compgs: Smaller and faster gaussian splatting with vector quantization. *ECCV*, 2024. 2
- [27] Simon Niedermayr, Josef Stumpfegger, and Rüdiger Westermann. Compressed 3d gaussian splatting for accelerated novel view synthesis. In *CVPR*, pages 10349–10358, 2024. 2
- [28] Maxime Oquab, Timothée Darcet, Théo Moutakanni, Huy Vo, Marc Szafraniec, Vasil Khalidov, Pierre Fernandez, Daniel Haziza, Francisco Massa, Alaaeldin El-Nouby, et al. Dinov2: Learning robust visual features without supervision. *arXiv preprint arXiv:2304.07193*, 2023. 3, 5

- [29] Jeong Joon Park, Peter Florence, Julian Straub, Richard Newcombe, and Steven Lovegrove. DeepSDF: Learning continuous signed distance functions for shape representation. In *CVPR*, pages 165–174, 2019. 2
- [30] Konstantinos Rematas, Andrew Liu, Pratul P Srinivasan, Jonathan T Barron, Andrea Tagliasacchi, Thomas Funkhouser, and Vittorio Ferrari. Urban radiance fields. In *CVPR*, pages 12932–12942, 2022. 1, 2
- [31] Weining Ren, Zihan Zhu, Boyang Sun, Jiaqi Chen, Marc Pollefeys, and Songyou Peng. Nerf on-the-go: Exploiting uncertainty for distractor-free nerfs in the wild. In *CVPR*, pages 8931–8940, 2024. 2, 3, 5, 7
- [32] Viktor Rudnev, Mohamed Elgharib, William Smith, Lingjie Liu, Vladislav Golyanik, and Christian Theobalt. Nerf for outdoor scene relighting. In *ECCV*, pages 615–631. Springer, 2022. 1, 2
- [33] Sara Sabour, Suhani Vora, Daniel Duckworth, Ivan Krasin, David J. Fleet, and Andrea Tagliasacchi. Robustnerf: Ignoring distractors with robust losses. In *CVPR*, pages 20626–20636, 2023. 3
- [34] Sara Sabour, Lily Goli, George Kopanas, Mark Matthews, Dmitry Lagun, Leonidas Guibas, Alec Jacobson, David J. Fleet, and Andrea Tagliasacchi. SpotLessSplats: Ignoring distractors in 3d gaussian splatting. *arXiv:2406.20055*, 2024. 3
- [35] Johannes L Schonberger and Jan-Michael Frahm. Structure-from-motion revisited. In *CVPR*, pages 4104–4113, 2016. 3, 1
- [36] Noah Snavely, Steven M Seitz, and Richard Szeliski. Photo tourism: exploring photo collections in 3d. In *SIGGRAPH*, pages 835–846. ACM, 2006. 5, 6, 7, 8, 3, 4
- [37] Cheng Sun, Min Sun, and Hwann-Tzong Chen. Direct voxel grid optimization: Super-fast convergence for radiance fields reconstruction. In *CVPR*, pages 5459–5469, 2022. 2
- [38] Matthew Tancik, Ethan Weber, Evonne Ng, Ruilong Li, Brent Yi, Terrance Wang, Alexander Kristoffersen, Jake Austin, Kamyar Salahi, Abhik Ahuja, et al. Nerfstudio: A modular framework for neural radiance field development. In *SIGGRAPH*, pages 1–12. ACM, 2023. 1, 2
- [39] Yuze Wang, Junyi Wang, and Yue Qi. WE-GS: An in-the-wild efficient 3d gaussian representation for unconstrained photo collections. *arXiv preprint arXiv:2406.02407*, 2024. 1
- [40] Zhou Wang, Alan C Bovik, Hamid R Sheikh, and Eero P Simoncelli. Image quality assessment: from error visibility to structural similarity. *IEEE TIP*, 13(4):600–612, 2004. 5, 1
- [41] Congrong Xu, Justin Kerr, and Angjoo Kanazawa. Splatfacto-w: A nerfstudio implementation of gaussian splatting for unconstrained photo collections. *arXiv preprint arXiv:2407.12306*, 2024. 2
- [42] Jiacong Xu, Yiqun Mei, and Vishal M. Patel. Wild-GS: Real-time novel view synthesis from unconstrained photo collections. In *NeurIPS*, 2024. 2, 5, 1
- [43] Qiangeng Xu, Zexiang Xu, Julien Philip, Sai Bi, Zhixin Shu, Kalyan Sunkavalli, and Ulrich Neumann. Point-nerf: Point-based neural radiance fields. In *CVPR*, pages 5438–5448, 2022. 1
- [44] Yifan Yang, Shuhai Zhang, Zixiong Huang, Yubing Zhang, and Mingkui Tan. Cross-ray neural radiance fields for novel-view synthesis from unconstrained image collections. In *ICCV*, pages 15901–15911, 2023. 1, 2, 3
- [45] Zehao Yu, Anpei Chen, Binbin Huang, Torsten Sattler, and Andreas Geiger. Mip-splatting: Alias-free 3d gaussian splatting. In *CVPR*, pages 19447–19456, 2024. 1, 2
- [46] Zehao Yu, Torsten Sattler, and Andreas Geiger. Gaussian opacity fields: Efficient and compact surface reconstruction in unbounded scenes. *ACM TOG*, 43(6):1–13, 2024. 1, 2
- [47] Dongbin Zhang, Chuming Wang, Weitao Wang, Peihao Li, Minghan Qin, and Haoqian Wang. Gaussian in the wild: 3d gaussian splatting for unconstrained image collections. *ECCV*, 2024. 2, 5, 6, 7, 1
- [48] Richard Zhang, Phillip Isola, Alexei A Efros, Eli Shechtman, and Oliver Wang. The unreasonable effectiveness of deep features as a perceptual metric. In *CVPR*, pages 586–595, 2018. 5, 1
- [49] Matthias Zwicker, Hanspeter Pfister, Jeroen Van Baar, and Markus Gross. Ewa splatting. *IEEE TVCG*, 8(3):223–238, 2002. 2, 3

NexusSplats: Efficient 3D Gaussian Splatting in the Wild

Supplementary Material

Overview

This appendix provides comprehensive documentation to support the claims and analyses in the main paper. It includes:

- **Supplementary videos** demonstrating real-time rendering, dynamic lighting adaptation, and occlusion handling.
- **Implementation specifics** including network architectures, training protocols, and hyperparameters.
- **Further experimental results** on additional scenes and ablation studies.
- **Visualizations** elucidating hierarchical light decoupling and occlusion handling.

These materials collectively strengthen the validation of NexusSplats while addressing practical reproducibility concerns.

Reproducibility

To ensure full reproducibility, we have included our **source code** in the supplemental material and released our open-source implementation on GitHub, including step-by-step instructions for scene reconstruction and rendering, and pre-trained models for Photo Tourism and NeRF On-the-go datasets. Training is typically completed within 6–8 hours on an NVIDIA A40 GPU.

Video Demo

The supplementary videos provide dynamic, real-time demonstrations that extend beyond the static figures in the main paper. They showcase NexusSplats’ capabilities across two dimensions: multi-view renderings under varying lighting conditions and interactive side-by-side comparisons with 3DGS [12], GS-W [47], and WildGauss [14] in complex outdoor environments. These visualizations highlight our method’s unique strengths — particularly its ability to harmonize lighting adaptation with geometric precision while maintaining real-time performance. We strongly encourage readers to watch these videos to fully appreciate the temporal coherence of reconstructed scenes.

A. Implementation Details

Our implementation initializes *nexus kernels* from Structure-from-Motion (SfM) points [35], aligning with established practices in neural scene representation [12, 23, 43]. Each *nexus kernel* manages $h = 10$ neural Gaussians through learnable offsets, with a 32-dimensional local context feature vector \mathbf{f}_u to encode spatial semantics, consistent with Scaffold-GS [20]. Kernel pruning

Table 3. **Overfitting Studies** on the Sacre Coeur scene, where the performance in quality drops the most, showing the results of different dropout rates in the light decoupling module. **Bold** indicates best results.

Dropout Rate	PSNR \uparrow	SSIM \uparrow	LPIPS \downarrow
0	22.80	0.857	0.174
0.1	22.44	0.859	0.176
0.2	22.99	0.859	0.172
0.3	22.51	0.857	0.176
0.4	22.28	0.853	0.179
0.5	22.32	0.855	0.177

occurs between 1500 and 15000 iterations, removing underperforming kernels with accumulated opacity below $\tau = 0.005$.

For lighting adaptation, we adopt a 32-dimensional image-specific light embedding ε_l and a 30-dimensional kernel-wise appearance embedding ε_a . The color mapping MLP F_θ employs two 256-unit hidden layers with ReLU activations, while a dropout rate of 0.2 optimally balances generalization and overfitting (see Table 3).

Similarly, the uncertainty propagation module uses a 32-dimensional image-specific transient embedding ε_τ and a 30-dimensional kernel uncertainty embedding ε_σ , processed by an MLP F_σ with two 128-unit layers.

Training is conducted using PyTorch and Adam optimization, with evaluation performed via the NerfBaselines framework [13]. We excluded methods, including HA-NeRF [4], CR-NeRF [44], RefinedFields [11], SWAG [6], Wild-GS [42] and WE-GS [39], due to unavailable implementations or hardware constraints. We adhere strictly to dataset splits and metrics from [13] for fair comparisons.

B. Comparisons on NeRF On-the-go

While NexusSplats achieves state-of-the-art performance in large-scale outdoor scenes with coupled lighting and occlusion challenges, its quantitative results on the NeRF On-the-Go dataset — a benchmark focusing on small-scale indoor scenes with graded occlusion levels — lag behind specialized baselines like WildGauss [14]. This discrepancy stems from two factors inherent to our design priorities and evaluation metrics.

First, traditional metrics like PSNR, SSIM [40], and LPIPS [48] measure global photometric fidelity rather than occlusion-specific accuracy. As shown qualitatively in Figure 7, our method successfully removes transient occlusions

Table 4. **Quantitative Comparison** on the NeRF On-the-go dataset [31]. Highlighted values indicate the first, second, and third scores for each metric and scene.

Method	Low Occlusion						Medium Occlusion						High Occlusion					
	Mountain			Fountain			Corner			Patio			Spot			Patio-High		
	PSNR ↑	SSIM ↑	LPIPS ↓	PSNR ↑	SSIM ↑	LPIPS ↓	PSNR ↑	SSIM ↑	LPIPS ↓	PSNR ↑	SSIM ↑	LPIPS ↓	PSNR ↑	SSIM ↑	LPIPS ↓	PSNR ↑	SSIM ↑	LPIPS ↓
3DGS [12]	19.87	0.648	0.200	20.21	0.661	0.183	20.75	0.722	0.242	17.27	0.700	0.204	19.04	0.628	0.433	17.24	0.599	0.365
GS-W [47]	19.39	0.599	0.301	18.88	0.599	0.264	22.69	0.802	0.148	20.92	0.776	0.148	16.92	0.606	0.415	19.42	0.684	0.253
WildGauss [14]	20.90	0.673	0.233	20.92	0.672	0.210	23.46	0.810	0.157	21.27	0.805	0.134	24.02	0.781	0.162	21.89	0.736	0.203
Ours	20.04	0.645	0.287	20.59	0.649	0.243	23.41	0.809	0.147	20.08	0.767	0.169	22.64	0.762	0.198	20.92	0.704	0.253

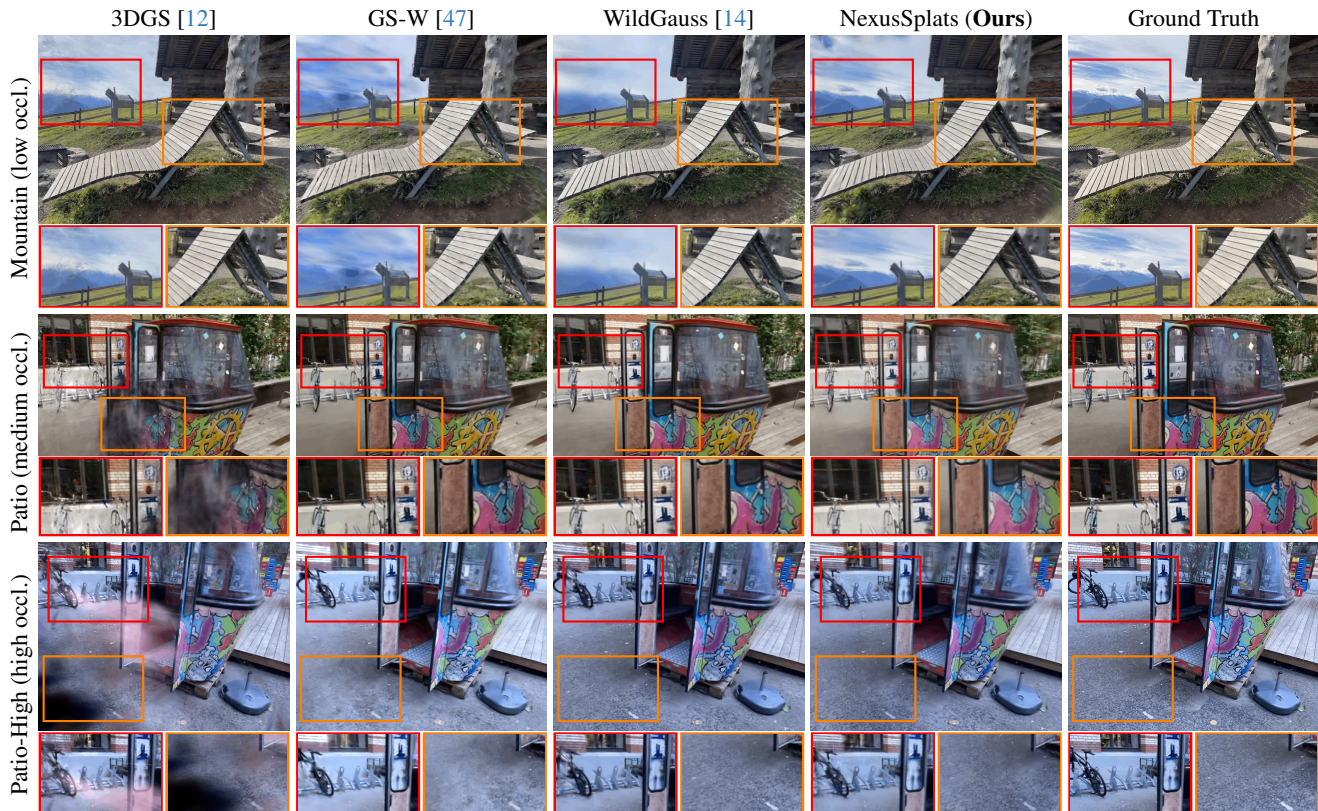


Figure 7. **Qualitative Comparison** on the NerRF On-the-go dataset [31]. We present the results of the remaining three scenes.

(e.g. moving objects in "Patio-High") but incurs slight blurring in boundary regions. NexusSplats prioritizes occlusion robustness over high-frequency detail preservation in small-scale indoor settings.

Second, the hierarchical representation [20], tailored for efficient large-scale scene reconstruction via voxel-aligned kernels, struggles to resolve fine textures in confined indoor spaces. This architectural bias toward outdoor scenarios leads to suboptimal parameter tuning for small-scale geometry. Nevertheless, our approach maintains competitive occlusion localization (e.g. 23.41 PSNR in "Corner" vs. WildGauss's 23.46) while requiring fewer parameters, underscoring its suitability for real-world applications

where efficiency and occlusion handling outweigh synthetic benchmark optimization. our future work will explore adaptive kernel scaling to bridge this domain gap without compromising outdoor performance.

C. Further Ablations and Visualizations

Qualitative Ablations on Photo Tourism. We visualize the impact of key components by progressively removing the hierarchical light decoupling module (w/o light.), uncertainty propagation (w/o uncert.), and boundary-aware refinement (w/o refine.). As shown in Figure 8, the full NexusSplats framework (rightmost column) restores pho-

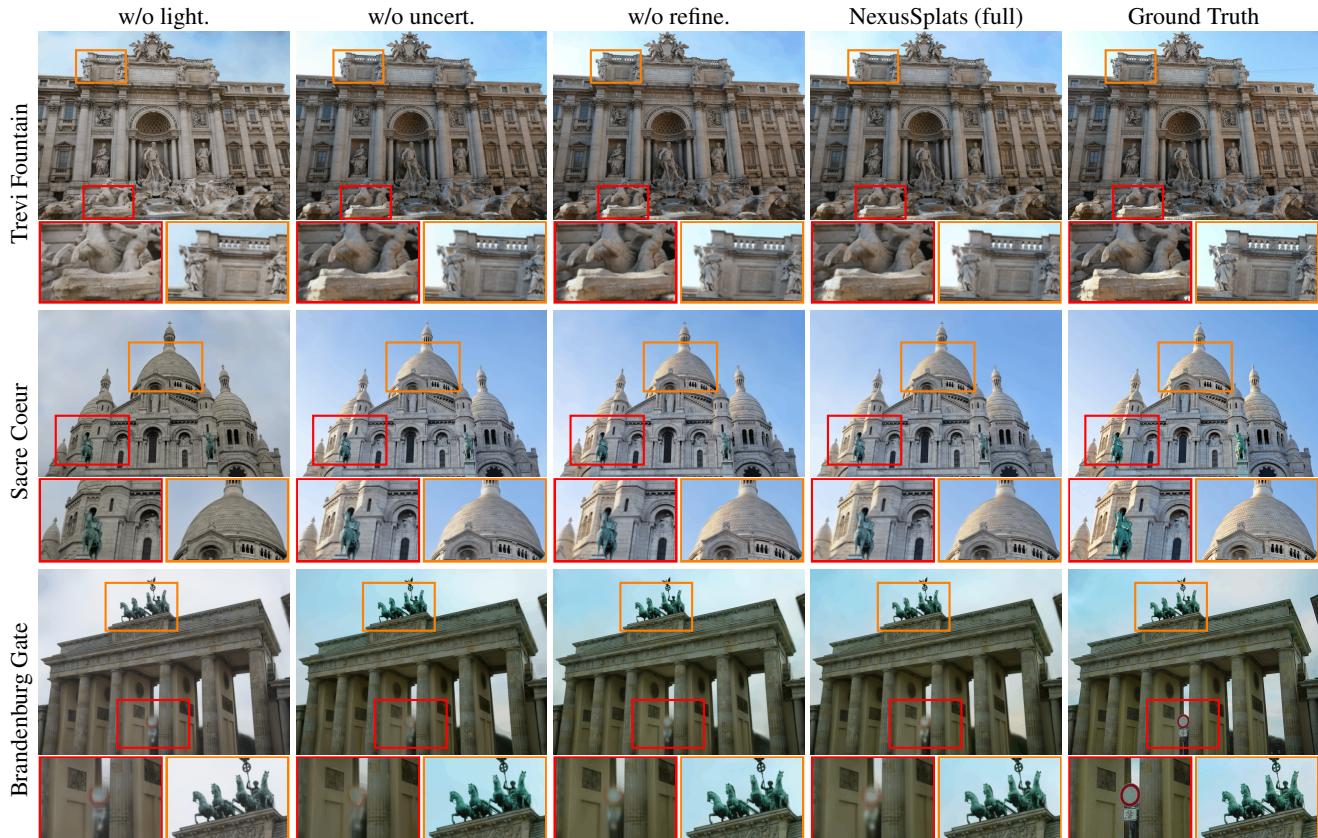


Figure 8. **Qualitative Ablations** on the Photo Tourism dataset [36].

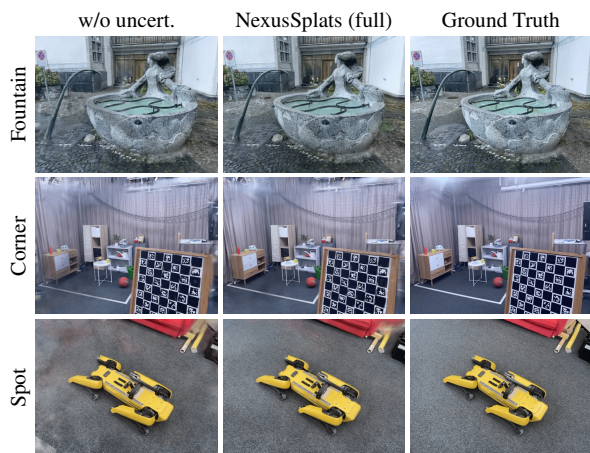


Figure 9. **Qualitative Comparison** on the NerRF On-the-go dataset [31].

tometric stability and geometric precision, closely matching ground truth. These visual comparisons underscore the necessity of all three modules for robust *in-the-wild* reconstruction.

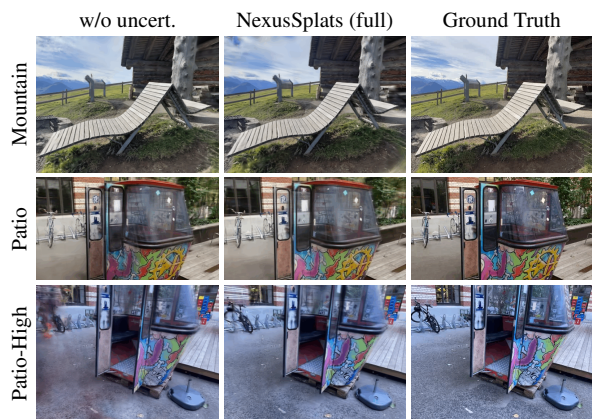


Figure 10. **Qualitative Comparison** on the NerRF On-the-go dataset [31].

Qualitative Ablations on NerRF On-the-go. Removing the uncertainty propagation module (w/o uncert.) severely impacts occlusion handling across diverse indoor scenes. In the Corner and Spot sequences, transient objects leave residual artifacts in rendered views, as the model fails to distinguish static structures from occlusions. The Spot scene exhibits blurred boundaries around furniture legs due to

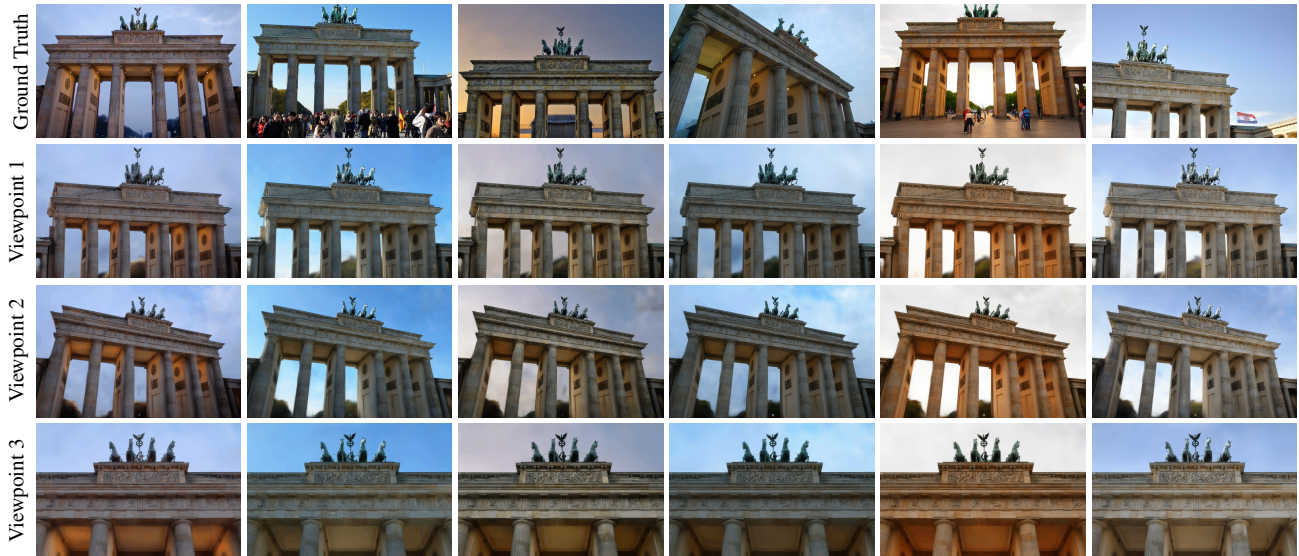


Figure 11. **Light Decoupling Visualization** for Brandenburg Gate.



Figure 12. **Light Decoupling Visualization** for Sacre Coeur.

unchecked uncertainty accumulation. Similarly, in outdoor-like setups (Mountain and Patio), missing uncertainty propagation learns occlusion geometries and erodes terrain details. The full NexusSplats framework restores precision while preserving intricate textures in partially observed areas. These results validate that our uncertainty propagation mechanism is indispensable for robustly aligning 3D geometry with 2D observations, particularly in scenes with dense transient elements or complex lighting interplay.

Light Decoupling Visualization. Figure 11 and Figure 12 evaluate the light decoupling performance of

NexusSplats on the remaining two scenes in the Photo Tourism dataset [36], Brandenburg Gate and Sacre Coeur, respectively. The results showcase our method’s ability to adapt reconstructed scene colors to match diverse target lighting conditions derived from the ground images. For each scene, six lighting conditions are visualized from three different viewpoints. The consistent adaptation across lighting conditions highlights the effectiveness of the light decoupling module in generalizing across scenes and conditions.

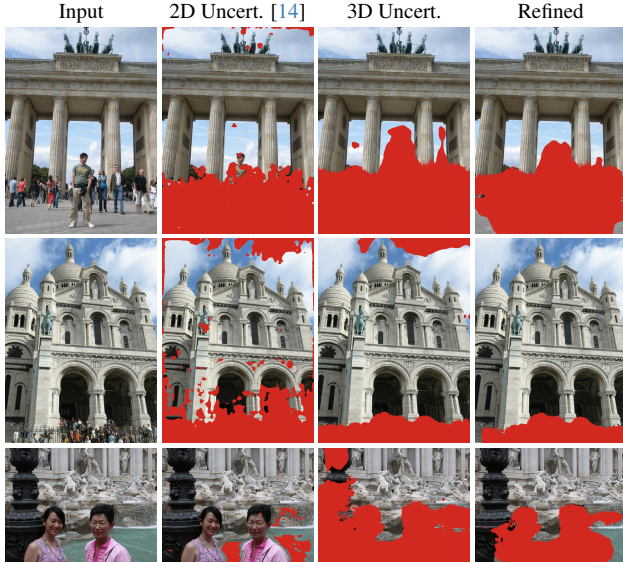


Figure 13. Additional **Uncertainty Handling Visualization** for three scenes from the Photo Tourism dataset [36].

Uncertainty Splatting Visualization. Figure 13 presents additional visualization results of uncertainty predictions, highlighting our method’s ability to accurately capture occlusions.

D. Discussions and Limitations

While NexusSplats significantly improves occlusion handling through 3D uncertainty propagation and boundary-aware refinement, its current formulation exhibits limitations in scenarios requiring fine-grained scene completion. Excluding occluded pixels from the optimization process inherently halts color learning in masked regions, occasionally introducing visible gaps or artifacts in rendered views — a trade-off inherent to occlusion-filtering frameworks.

This issue is exacerbated in densely occluded urban scenes, where transient objects mask large contiguous areas, leaving under-optimized “holes” that degrade perceptual quality. A promising remedy lies in integrating image inpainting techniques, such as masked autoencoders [10] or diffusion models, to hallucinate plausible textures in excluded regions while preserving geometric consistency.

Additionally, while our hierarchical kernel design excels in large-scale outdoor scenes, it struggles to resolve intricate details in confined indoor environments (e.g. scenes in the NeRF On-the-Go dataset), where high-density representations demand finer-grained spatial partitioning. This limitation stems from the kernel pruning process, which prioritizes computational efficiency over adaptability to varying scene scales.

Future work could explore more robust and scalable kernel optimization to bridge this gap. Despite these chal-

lenges, NexusSplats achieves a critical balance: it pioneers efficient, structure-aware occlusion handling without compromising the core advantages of 3DGS — real-time rendering and photorealistic quality — in its target domain of *in-the-wild* scene reconstruction.